Neutron reflection study of the interaction of the eukaryotic pore-forming actinoporin equinatoxin II with lipid membranes reveals intermediate states in pore formation

Hanna P. Wacklin, Biserka Bakrač Bremec, Martina Moulin, Nejc Rojko, Michael Haertlein, Trevor Forsyth, Gregor Anderluh, Raymond S. Norton

PII: S0005-2736(15)00417-4
DOI: doi: 10.1016/j.bbamem.2015.12.019
Reference: BBAMEM 82078

To appear in: *BBA - Biomembranes*

Received date: 4 March 2015
Revised date: 2 November 2015
Accepted date: 15 December 2015

Please cite this article as: Hanna P. Wacklin, Biserka Bakrač Bremec, Martina Moulin, Nejc Rojko, Michael Haertlein, Trevor Forsyth, Gregor Anderluh, Raymond S. Norton, Neutron reflection study of the interaction of the eukaryotic pore-forming actinoporin equinatoxin II with lipid membranes reveals intermediate states in pore formation, *BBA - Biomembranes* (2015), doi: 10.1016/j.bbamem.2015.12.019

Neutron reflection study of the interaction of the eukaryotic pore-forming actinoporin equinatoxin II with lipid membranes reveals intermediate states in pore formation

Hanna P. Wacklin[1-3], Biserka Bakrač Bremec[4], Martina Moulin[3], Nejc Rojko[4,5], Michael Haertlein[3], Trevor Forsyth[3,6], Gregor Anderluh[4,5,*] and Raymond S. Norton[6,7,*]

[1] *European Spallation Source ESS AB, P.O. Box 176, 221 00 Lund, Sweden*

[2] *Nanoscience Center and Institute of Chemistry, Copenhagen University, Universitetsparken 5, DK-2100 Copenhagen E, Denmark*

[3] *Institut Laue-Langevin, BP 156, 38042 Grenoble, France*

[4] *Department of Biology, Biotechnical Faculty, University of Ljubljana, Jamnikarjeva 101, 1000 Ljubljana, Slovenia*

[5] *Laboratory for Molecular Biology and Nanobiotechnology, National Institute of Chemistry, Hajdrihova 19, 1000 Ljubljana, Slovenia*

[6] *Faculty of Natural Sciences, Keele University, Staffordshire ST5 5BG, United Kingdom*

[7] *Medicinal Chemistry, Monash Institute of Pharmaceutical Sciences, Monash University, Parkville, Victoria 3052, Australia*

Keywords: cytolysin; equinatoxin II, pore formation; membrane; neutron reflection, sphingomyelin, cholesterol

Running title: Membrane binding of equinatoxin II

[*] Corresponding authors:

Gregor Anderluh: Laboratory for Molecular Biology and Nanobiotechnology, National Institute of Chemistry, Hajdrihova 19, 1000 Ljubljana, Slovenia. Phone +386 1 476 02 61. Fax: +386 1 476 03 00. Email: gregor.anderluh@ki.si

Ray Norton: Medicinal Chemistry, Monash Institute of Pharmaceutical Sciences, Monash University, Parkville, Victoria 3052, Australia. Phone +61 3 9903 9167. Fax: +61 3 9903 9582. Email: ray.norton@monash.edu

Abbreviations: Chol, cholesterol; DHPC, dihexanoyl-phosphatidylcholine; DMPC, dimyristoyl-phosphatidylcholine; DTT, dithiothreitol; EqtII, equinatoxin II; PC, phosphatidylcholine; SM, sphingomyelin; StII, sticholysin II; SUV, small unilamellar vesicles

Abstract

Equinatoxin II (EqtII), a eukaryotic pore-forming toxin, lyses cell membranes through a mechanism involving the insertion of its N-terminal α-helix into the membrane. EqtII pore formation is dependent on sphingomyelin (SM), although cholesterol (Chol) and membrane microdomains have also been suggested to enhance its activity. We have investigated the mechanism of EqtII binding and insertion by using neutron reflection to determine the structures of EqtII-membrane assemblies *in situ*. EqtII has several different modes of binding to membranes depending on the lipid composition. In pure dimyristoyl-phosphatidylcholine (DMPC) membranes, EqtII interacts weakly and reversibly with the lipid head groups in an orientation approximately parallel to the membrane surface. The presence of sphingomyelin (SM) gives rise to a more upright orientation of EqtII, but Chol is required for insertion into the core of the membrane. Cooling the EqtII-lipid assembly below the lipid phase transition temperature leads to deep water penetration and a significant reduction in the extension of the protein outside the membrane, indicating that phase-separation plays a role in EqtII pore-formation. An inactive double-cysteine mutant of EqtII in which the α-helix is covalently tethered to the rest of the protein, interacts only reversibly with all the membranes. Releasing the α-helix in situ by reduction of the disulphide bridge, however, causes the mutant protein to penetrate in DMPC-SM-Chol membranes in a manner identical to the wild-type protein. Our results help clarify the early steps in pore formation by EqtII and highlight the valuable information on protein-membrane interactions available from neutron reflection measurements.

Keywords: Equinatoxin II, Pore formation, Neutron reflection, Sphingomyelin, Cholesterol, Deuteration

1. Introduction

Equinatoxin II and other actinoporins are highly basic 20-kDa proteins that display cytolytic activity in model lipid and cell membranes that is markedly enhanced by sphingomyelin (SM) [1-3]. They differ from other classes of bacterial pore-forming toxins [4] in that they are smaller, more potent, stable to proteolytic degradation, and form a pore that does not have a stable structure and that has not yet been visualized directly [5]. Actinoporin pores have a radius of about 1 nm [6-9] and are permeable to small molecules and solutes, with the resulting osmotic imbalance promoting cell lysis. These oligomeric pores formed in various lipid membranes have been reported to consist of three or, more likely, four monomers [6, 10-12]. Tetramers of the actinoporin sticholysin II (StII) have been observed both in solution [7] and when crystallized on lipid monolayers [13]. Crystallographic and cryo-EM studies of fragaceatoxin C, in contrast, suggested that this actinoporin formed octameric or nonameric pore structure [14, 15], but it remains to be seen if these observations apply to other members of this family.

SM plays a key role in the lytic activity of the actinoporins. The haemolytic activity of an actinoporin from *Stichodactyla helianthus* is inhibited by pre-incubation with SM, and treatment of erythrocyte membranes with sphingomyelinase renders them resistant to lysis [16, 17]. More recent studies with sticholysins I [10] and II [18] on model membranes confirmed that SM in the membrane enhances lytic activity and suggested that Chol may have a minor role [18]. The haemolytic activity of tenebrosin C[19], which was isolated from the Australian red waratah sea anemone *Actinia tenebrosa* and proved to be identical to equinatoxin II (EqtII) from *Actinia equina L.* [20, 21], was also inhibited by pre-incubation with SM [22]. The molecular details of the interaction of EqII with SM [23] have been studied extensively [24]. Direct binding assays employing lipid dot blots and surface plasmon resonance experiments showed that EqtII specifically recognizes SM but not other lipids. The presence of SM in membranes improved both the binding and permeabilizing activity of EqtII [24]. Analysis of the interfacial binding site predicted that the two most important residues for SM recognition are Trp112 and Tyr113, and that electrostatic interactions play a minor role in membrane interactions [24, 25]. A similar association of SM with the head group binding site was recently proposed for StII based on binding assays employing SM analogues and molecular modelling [25].

The structure of EqtII [26] solved in solution [27, 28] and by X-ray crystallography [29], consists of two short helices packed against opposite faces of a β-sandwich structure formed by two five-stranded β-sheets. Several approaches have been pursued in an effort to elucidate the molecular mechanism of pore formation by actinoporins. Small increases in the β-sheet and α-helical content of EqtII in unilamellar vesicles were detected by CD and FTIR [8, 30, 31]. The N-terminal region (residues 10-28) [32, 33] and the surface aromatic cluster including Trp112 and 116 were found to embed in lipid membranes [32, 34, 35]. Based on these findings, it has been proposed that EqtII binds to membranes initially via the aromatic residues, followed by interaction of the N-terminus with the lipid membrane surface [36] and finally translocation across the bilayer [37] to form a functional pore [38, 39].

Despite considerable progress in understanding EqtII-lipid interactions, the structural details of the EqtII-membrane assembly during the pore formation process are not well understood. Neutron reflection [40] allows the depth of proteins [41] or nucleic acids [42, 43] to be determined in supported planar membranes on the nanometre scale [44], as well as the structural changes induced in the membrane *in situ*. In addition, selective deuterium labelling of the lipids allows the membrane composition to be determined directly and related to the protein activity [45]. Neutron reflection has been used to elucidate the structure of membrane protein-receptor complexes [46], toxin penetration [47] and ion channel structure [48] in membranes. In this study we use neutron reflection to investigate the initial binding mechanism of EqtII to membranes containing SM and Chol. We show that, while wild-type EqtII is able to associate with pure DMPC membranes, its orientation changes in the presence of SM, and Chol is required for deep penetration of the protein into the hydrophobic core of the membrane. The deep penetration into SM- and Chol-containing membranes occurs at lipid compositions outside the domain coexistence region without observable open pore formation, consistent with the role proposed for lipid domains in pore formation. In contrast, an oxidized double-cysteine mutant of EqtII, in which the dissociation of the α-helix from the β-sandwich is prevented [35, 39] binds to membranes in a partly reversible manner, and shows no penetration until the α-helix is released *in situ* by the reducing agent dithiothreitol (DTT).

2. Materials and methods

2.1. Materials

Chain deuterated 1,2-D_{54}-dimyristoyl-*sn*-glycero-3-phosphocholine (D_{54}-DMPC), 1,2-dimyristoyl-*sn*-glycero-3-phosphocholine (DMPC), egg sphingomyelin (SM), and cholesterol (Chol) were purchased from Avanti Polar Lipids (Alabaster, AL), Tris-HCl, NaCl and DTT were from Sigma Aldrich and D_2O (>99%) was provided by the Institut Laue Langevin, Grenoble.

2.2. Expression and Purification of Proteins

Wild-type EqtII and the double cysteine mutant EqtII^{V8C,K69C} (in which residues at positions 8 and 69 are replaced by cysteine) were expressed in *E. coli* [35, 49]. *E. coli* growth in a 100% D_2O medium combined with a fully deuterated carbon source allows the expression of fully (100%) perdeuterated recombinant proteins in a reproducible and predictable manner [50]. Optimization of the soluble expression level and large scale production of fully deuterated recombinant EqtII and EqtII^{V8C,K69C} was carried out in the ILL-EMBL deuteration laboratory [51, 52] using the same protocol as recombinant myoglobin, for which the deuteration level was shown to be very close to 100% by mass spectroscopy [53]. *E. coli* BL21(DE3) was transformed with a pT7-7 based expression vector coding for the wild-type or EqtII^{V8C,K69C} [35]. Cells were grown in deuterated minimal medium with perdeuterated D_8-glycerol (Euriso-Top, France) as a carbon source; adaptation of BL21(DE3) cells to deuterated minimal medium was achieved by a multi-stage adaptation process [54]. 1.5 L of deuterated medium was inoculated with 100 mL culture of adapted cells in a 3 L fermenter (Labfors, Infors). During the batch and fed-batch phases the pH was adjusted to 6.9 (by addition of NaOD) and the temperature was adjusted to 30 °C. The gas-flow rate of sterile-filtered air was 0.5 L min^{-1}. Stirring was adjusted to ensure a dissolved oxygen tension of 30 %. The fed-batch phase was initiated when the optical density at 600 nm reached 3.2. D_8-glycerol was added to the culture to keep the growth rate stable during fermentation. When OD_{600} reached 13 (10.5 for the mutant), protein expression was induced by the addition of 1 mM IPTG and incubation continued for 24 h. Cells were harvested at an OD_{600} of 16, washed with 10 mM HEPES (pH 6.4), and stored at -80 °C. About 60 g of perdeuterated cell paste was obtained for each of the expression constructs. Proteins were purified from the cells as described previously [35, 49].

2.3. Protein purity and activity

The quality of the protein preparations was verified by SDS-PAGE (Fig. S1, Supplementary material). The activities of the deuterated and non-deuterated wild-type proteins were virtually identical, as measured by haemolysis of bovine erythrocytes. The oxidised from of the double cysteine mutant EqtII^{V8C,K69C} (EqtII^{V8C,K69C}O) showed no activity towards erythrocytes, but the reduced form (EqtII^{V8C,K69C}R) shows full activity (Fig. S2, Supplementary material).

2.4. Supported membrane formation

The support surfaces (single crystal silicon cut along the (111) crystal plane) were cleaned for 15 min in a 1:4:5 solution of H_2O_2:H_2SO_4:H_2O at 80 ºC followed by UV ozonolysis for 5-10 min before the experiment. This treatment generates a highly hydrophilic SiO_2 layer of 7-15 Å thickness and 3-8 Å surface roughness [55].

Small unilamellar vesicles (30-50 nm) were prepared by sonication as described previously [45, 56]. In brief, lipid suspensions in chloroform were mixed in appropriate ratios and the solvent was then evaporated under a stream of N_2. The resulting dry lipid films were suspended in 100 mM NaCl in D_2O at a concentration of 0.5 mg/mL and incubated for at least 30 min at 45 °C before sonication. Sonication was performed with a tip sonicator until a clear solution was obtained, typically over 8-12 min with a 50% duty cycle (15 s on/off).

Supported phospholipid bilayers were formed by vesicle fusion to a silicon substrate pre-heated to 55 °C with an incubation period of 20-30 min prior to rinsing off the excess vesicles with 100 mM NaCl, followed by rinsing in 10 mM Tris buffer (pH 7.4) and cooling to 30 °C. All protein adsorption experiments were carried out at 30 °C unless otherwise specified.

2.5. Neutron reflection

Specular neutron reflection [40] was measured on the D17 reflectometer [57] at the Institut Laue Langevin, Grenoble, using neutron wavelengths λ of 2-20 Å to record reflectivity R = I_0/I_R profiles between $0.01 < Q < 0.25$ Å^{-1}, where $Q = 4\pi\sin\Theta/\lambda$ is the momentum transfer vector of the neutrons in the direction (z) perpendicular to the membrane-water interface, and the reflectivity R is the ratio of the reflected intensity I_R to the incident intensity I_0. Under these conditions a typical measurement at two incident angles (0.7 º and 3.0 º) was used to obtain the full reflectivity profiles. The phospholipid bilayers were formed *in situ* in the neutron reflectometer sample chamber after measuring the reference structure of the

underlying Si-SiO_2 surface in D_2O and H_2O. Each lipid membrane structure was also measured in the same two contrasts before exposure to the proteins. Contrast changes were achieved by rinsing with 20 mL of the solvent. The slight variation in the SLD values of the bulk H_2O and D_2O are due to 90-100% efficiency of the solvent exchange process (the values are listed in the Supplementary material tables). Protein solutions (3 mL) in 10 mM Tris pH 7.4 were injected over the lipid membranes at either 0.1 mg/mL, or stepwise at increasing concentrations (0.05, 0.25, 0.5 mg/mL), and changes in reflectivity were recorded at 10 min intervals at the first angle of incidence (0.7 °) for 30 min to observe any time-dependence before recording the final reflectivity profile at both angles in two contrasts. No change was observed between the 10 min measurements, and therefore the structure had already reached a time-independent state before the measurements were started. In experiment with the double cysteine mutant $EqtII^{V8C,K69C}$, DTT at a final 2 mM concentration was injected after protein binding to release the disulphide bond between the α-helix and β-sandwich.

Details of the analysis of supported lipid membrane structure [58] and interaction with soluble proteins [59] using time-of-flight neutron reflection have been described in detail previously. Briefly, the neutron scattering length density profile ρ(z) of a lipid bilayer can be described by distinct regions corresponding to the polar head groups and hydrophobic acyl chains due to their chemical differences. Reflectivity analysis is based on modelling the thickness, scattering length density, solvent volume fraction, and interfacial roughness of typically three layers corresponding to the lipid head groups and the acyl chain region. In membranes containing lipids, water and a protein, the scattering length density ρ_{layer} is the sum of the molecular scattering length densities of the components ρ_i weighted by their volume fractions ϕ_i:

$$\rho_{layer} = \phi_{lipid}\rho_{lipid} + \phi_{water}\rho_{water} + \phi_{protein}\rho_{protein}$$

Thus, when there are significant differences in the molecular scattering length densities of lipid, protein and water, their volume fractions can be computed from the fitted scattering length density profile of the membrane by using contrast variation. Varying the solvent D_2O content allows the solvent volume fraction in the membrane to be determined. We additionally used lipids with deuterated (D-lipids) and non-deuterated (H-lipids) chains and proteins to detect the protein penetration independently from water penetration into the bilayers.

Fig. 1 shows the different scattering contrasts used for lipid bilayers interacting with EqtII. For each membrane composition, the experiments were repeated up to eight times: H-lipids + H-EqtII, H-lipids + D-EqtII, D-lipids +H-EqtII and D-lipids + D-EqtII, each combination in pure H_2O and pure D_2O solvents respectively. The colouring in Fig. 1 illustrates the sensitivity of each contrast to different features of the structure. The Motofit program [60] was used for optical matrix modelling to calculate neutron reflectivity from these model structures, as described in the Supplementary Material. For each membrane, the fits to both solvent contrasts were refined in a simultaneous analysis until a global fit to the experimental data was found. Each parameter was fitted within limits chosen from a physically realistic parameter space considering the lipid molecular details (e.g. that the lipid chains could not be longer than the all-trans length of the chain). The fits were constrained by the requirement that the area per molecule derived from the fitted thickness and volume fraction had to be constant for the lipid head groups and chains to within the fitting errors. For the several individual samples formed to obtain all measured contrasts, the data were fitted to global trends in the type of structure formed, while relaxing the absolute requirement on a global structure. The values listed in the tables of results are the average values from all sample formed. The individual sample structures are listed in the Supplementary material.

The scattering length densities of the phospholipids were calculated from volume fractions of the lipid components obtained from molecular dynamics simulations benchmarked against experimental data [61] and for the proteins they were calculated from the sequences and amino acid volumes determined in solution [62], assuming that protons on polar residues are exchangeable with the solvent, giving both deuterated and non-deuterated EqtII a different scattering length density in H_2O and D_2O solvents. Considering the limited experimental resolution to the thickness and volume fraction of protein layers with a high solvent content, as is the case for EqtII, a uniform scattering length density was used to describe the protein instead of a detailed profile derived by projections of the crystal structure in different orientations [48]. The penetration and volume fraction of EqtII (% EqtII) in the lipid bilayer were derived from the changes to the fitted lipid scattering length density compared to the values for the pure lipid. The values used for the lipids and proteins are listed in Table S1 (Supplementary material). The errors in the structural parameters were derived from the maximum acceptable variation in each fitted parameter (thickness, scattering length density and lipid volume fraction) that allowed a fit to all contrasts to be maintained, as described in

more detail in the Supplementary material. The errors in independent parameters of the model sublayers are coupled in such a way that the overall errors in membrane lipid volume fraction and thickness are ±10% and ±2 Å, respectively. The uncertainty in the penetration depth of the protein corresponds to the uncertainty in fitting the thickness of the lipid headgroups and/or lipid chain layers. A more detailed penetration model was not considered, as the small amounts of protein do not allow the penetration depth to be resolved in greater detail.

3. Results

To determine protein location and possible pore formation, the interactions of both wild-type EqtII and EqtII^{V8C,K69C} with three different types of membranes were characterised using several isotopic contrasts with deuterated (D-EqtII) and non-deuterated (H-EqtII) versions of both proteins, and deuterated (D-lipids) and non-deuterated (H-lipids) DMPC in two different solvent contrasts (H_2O and D_2O), as shown in Fig. 1. The EqtII concentrations in solution were 0.1 mg/mL (5.0 μM) unless otherwise stated. The full model structures fitted to all lipid bilayers are described in the Supplementary material.

3.1. Structure of lipid bilayers

Lipid bilayers were prepared from pure DMPC, DMPC containing sphingomyelin (SM) and DMPC containing both SM and Chol. The main structural parameters, averaged over all bilayers prepared, measured before the introduction of EqtII are shown in Table 1. The lipid volume fraction in the bilayers prepared varied between 0.92 and 0.96, showing that the formation from sonicated vesicles is very reproducible.

DMPC bilayers at 30 °C have a total thickness of 41±2 Å, with an average area per molecule of 62±5 Å^2, and a polar head group thickness of 7±1 Å. The 20 mol% and 30 mol% SM-containing bilayers are 44±2 Å thick, with the head group conformation extended to 8±1 Å with an increased solvent volume fraction of 34±3 v/v% compared to 19±3 v/v% in pure DMPC. There is a small difference in the headgroup conformation in the 20 mol% SM bilayer, with a slightly higher solvent fraction (40±10 v/v%) and thickness (9±1 Å) on the surface-proximal side compared to the headgroups facing the solution. Such a difference is often observed due to the additional water incorporated between the bilayer and the substrate due to the roughness of the silica surface (4-6 Å). The actual SM contents, as determined by fitting the neutron scattering length density of the lipid chains in D_{54}DMPC membranes, were 22±3 and 27±3 mol% for the nominal 20 and 30 mol% samples.

The presence of Chol increases the membrane thickness to 47±2 Å, with the lipid chain area per molecule decreasing to 57±4 $Å^2$. The scattering length density of the D_{54}-DMPC membrane with 20 mol% SM and 10 mol% Chol can be fitted to 3.8 x 10^{-6} $Å^{-2}$.

3.2. Binding of EqtII to DMPC Membranes

Wild-type EqtII binds very weakly to pure DMPC bilayers, as shown in Fig. 2a, in which the normalised neutron reflectivity profiles of the membranes before and after toxin injection show only modest changes. The structural parameters fitted to DMPC bilayers after EqtII interaction are summarized in Table 2. The structure of the hydrophobic membrane core is not altered by EqtII, which binds at the head group-water interface at 0.13±0.03 μmol m^{-2}. From the changes in the scattering length density model shown in Fig. 2b we can infer that the toxin penetrates into the phosphatidylcholine head groups, which have a thickness of 7±1 Å, and extends 15±3 Å above the surface of the membrane. The lipid head group scattering length density (1.8 x 10^{-6} $Å^{-2}$ for a DMPC head group) increases to 2.5 x 10^{-6} $Å^{-2}$ upon interaction with D-EqtII and to 2.0 x 10^{-6} $Å^{-2}$ with H-EqtII, which corresponds to 12.5±6% of the lipid head group volume being occupied by the protein. The dimensions of a single EqtII molecule have been reported to be 42 Å x 28 Å x 32 Å in the crystal structure [29]. Considering the low surface density of EqtII at the membrane surface, a layer with a homogeneous scattering length density was used to model the protein, instead of direct projections from the crystal structure [63]. As no specific deuterium label was attached to the N-terminal α-helix, it is not possible to say directly what its orientation relative to the membrane surface is, but the total protein layer thickness of 22±4 Å corresponds well to the shortest protein axis and indicates that only a single protein layer is partially embedded in the membrane, with a relatively parallel orientation of the protein long axis to the membrane surface. No change is observed in the lipid chain region that would indicate EqtII penetration or pore formation, to within the precision with which these can be determined from the fits (±3 v/v%), as demonstrated in Figures 2c and 2d. A similar procedure was applied to each fitting parameter to determine the uncertainties listed in Tables 1-5.

3.3. Binding of EqtII to SM-containing membranes

The structural parameters for EqtII in membranes containing 20 mol% and 30 mol% SM are summarized in Table 2, with the reflectivity data and scattering length density profiles shown in Fig. 3. The presence of SM significantly strengthens the EqtII-membrane

interaction, as evidenced by the higher surface coverage of protein (0.23±0.027 and 0.42±0.072 μmol m^{-2} for 20 and 30 mol% SM, respectively). Although a small change in the total scattering length density of the lipid chain region is observed, it can be attributed to the uncertainty in determining the solvent present in the tails (±0.05 v/v%); alternatively, the expulsion of a small amount of solvent when the protein binding to the lipid head groups leads to an area expansion of the lipids. There is no indication that EqtII penetrates into the hydrophobic lipid core or changes the overall membrane structure. EqtII interacts with the lipid head groups in a manner similar to that in pure DMPC in terms of the penetration depth (7±1 Å), but the thickness of the EqtII layer outside the membrane surface is on average 31±3 Å, twice the thickness on pure DMPC membranes, which, considering the ± 3 Å experimental error in determining the protein layer thickness, is a clear indication that the average orientation of the toxin is different. This reorientation at the membrane surface could be as a result of a different mode of binding through the SM-binding site. The residues involved in the SM interaction are located at the end of the longest axis of the protein [24, 25, 64], which would place the β-sandwich in a more upright orientation perpendicular to the membrane surface, consistent with the total protein layer thickness being 39±3 Å.

The volume fractions of EqtII in the lipid head groups and on the membrane surface are somewhat higher compared to pure DMPC. There is no difference in the protein layer thickness between 20 and 30 mol% SM, but both the amount of protein (0.42±0.0072 μmol m^{-2}) and the fraction of EqtII that penetrates into the lipid head groups is higher (37% relative to the lipid head group volume) for 30 mol% SM. The fraction of EqtII penetrating into the lipid head groups is comparable to the estimated volume of the α-helix relative to the rest of the protein based on NMR [28] (7%), synchrotron circular dichroism [65] (9±4%) or X-ray crystallography [29] (12%) studies. However, based on these data alone, we cannot infer that it is the helix that is embedded in the head groups and not another part of the protein..

3.4. Binding of EqtII to membranes containing SM and Chol

The interaction of EqtII was investigated with membranes containing 10 mol% Chol and 20 or 30 mol% SM, and as function of EqtII concentration. The structural parameters are summarised in Table 2, with the scattering length density profiles and corresponding model structures shown in Fig. 4.

The thickness and protein volume fraction of the EqtII layer on the surface of the lipid membrane are both similar to the membranes containing only DMPC and SM, but D-EqtII increases the chain scattering length density of the H-lipids from -0.3 x 10^{-6} $Å^{-2}$ to +0.12 x 10^{-6} $Å^{-2}$ in H_2O and to +0.59 x 10^{-6} $Å^{-2}$ in D_2O for 20 mol% SM and 10 mol% cholesterol. In the D-lipid bilayer, H-EqtII changes the chain scattering length density from 3.8 x 10^{-6} $Å^{-2}$ to 3.77 x 10^{-6} $Å^{-2}$ in H_2O and 3.66 x 10^{-6} $Å^{-2}$ in D_2O (see Supplementary material Table S4 for full details). The presence of Chol gives rise to penetration of EqtII across the hydrophobic lipid core, where the protein extends through to the opposing lipid head groups. However, there is no solvent penetration observed at either SM concentration, indicating that no open pores are formed. At 0.1 mg/mL EqtII, the protein volume fraction found in the lipid core is relatively low (10±2 %), and in the head groups it is similar to that found with SM only (11±3 %). Increasing the EqtII concentration to 0.5 mg/mL doubles the amount of protein outside the membrane surface, but leads to no further penetration into either the lipid head groups or lipid chains. Increasing the SM concentration to 30 mol% has only a moderate effect. The total protein amount bound to the membrane surface increases from 0.3 to 0.34 μmol m^{-2}, and the volume fraction of the protein volume penetrating into the lipid chains (15±5 %) and head groups (20±5 %) increases significantly more in the head groups. This implies that either the helix is not fully inserted, or that only some EqtII molecules at the membrane surface are able to penetrate into the lipid core.

When the membrane-EqtII assembly is cooled to 18 °C, which is below the liquid crystalline phase transition of both DMPC (24 °C) [66] and egg-SM (35-44 °C) [67], crossing the phase boundary into the gel-phase, the reflectivity profile changes substantially, corresponding to thickening of the membrane by 4±1 Å and significant water penetration (22 v/v% relative to the lipids) across the membrane, indicating that pore formation is enabled. Concurrently the protein layer outside the membrane shrinks from 35±3 Å to 16±3 Å in thickness, suggesting that in the pore, the orientation of the β-sandwich relative to the membrane changes to more parallel compared to the non-pore state.

The amount of EqtII bound to the surface of the membrane and penetrating into 10 mol% Chol and 20 mol% SM-containing membranes was determined as a function of EqtII concentration (Fig. 5a,b). The data suggest that the EqtII binding is already close to being saturated at 0.05 mg/ml as the changes that occur at higher concentrations mainly correspond to an increasing number of EqtII molecules penetrating the membrane, while it is difficult to

determine small changes in the protein layer outside the membrane as it contains only 5±3 v/v% protein. As can be seen from the changes in membrane structure in Table 4, EqtII penetrates into the lipid core already at 0.05 mg/mL concentration, and the amount of protein increases with EqtII concentration in solution, but even at 0.5 mg/mL EqtII in solution, no water penetration suggesting open pore formation is observed. This is consistent with the fact that, at the lipid compositions studied, the membranes do not form phase-separated domains, which have been shown to occur only at relatively high Chol (36 mol%) and SM (50 mol%) fractions with DMPC [68], as opposed to more unsaturated lipids such as POPC [69]. The main effect of increasing concentration is to increase the volume fraction of protein penetrating into both the lipid head groups and chains while both the penetration depth and the volume fraction of protein outside the membrane stay constant.

3.5. Binding of EqtII^{V8C,K69C} to membranes

To elucidate the role of the N-terminal α-helix in membrane binding of EqtII, we also investigated the binding of the double cysteine mutant EqtII^{V8C,K69C}O to DMPC, DMPC-SM and DMPC-SM-Chol membranes. The results are summarized in Table 5, with the changes in reflectivity and scattering length density profiles shown in Fig. 6. The scattering length density profiles in Fig 6 are convoluted with the surface roughness, which was in this case higher than in the other samples (8-16 Å), and as a consequence the SLD profiles do not describe only the lipid bilayer structure, for which the fitted structures can be found in the Supplementary material Tables S8-S10. The oxidized, inactive mutant binds to all membranes with a similar affinity to the wild-type protein, but with two key differences. The mutant protein layer outside the membrane surface is considerably thicker than for the wild-type protein on pure DMPC membranes, with the EqtII ^{V8C,K69C}O layer extending to 30±3 Å above the membrane, indicating that the mutant binds in a different orientation. In the presence of SM or both SM and Chol the mutant protein layer thickness outside the membrane is similar to that of wild-type EqtII, but binding of the mutant is partially reversible, with up to 50 % of the protein being washed off by a buffer rinse in all experiments. Such reversibility was not observed for the wild-type protein. Most importantly, the mutant only interacts with the lipid head groups in all cases, with no protein penetration into the lipid core. The small changes in lipid chain SLD listed in the Supplementary material tables are within the fitting uncertainty ($\pm$ 0.05 x 10^{-6} Å^{-2}).

When the α-helix is released *in situ* by the addition of 2 mM DTT, further changes in reflectivity are observed. In pure DMPC membranes, the addition of DTT only causes desorption of the protein, consistent with reversible binding of the wild-type protein with pure DMPC. In SM-containing membranes the mutant protein layer outside the membrane surface primarily becomes thinner upon DTT addition, with approximately 30 % of the protein removed, suggesting that the protein is partially reversibly bound. However, in the presence of Chol an irreversible penetration into the lipid chains is observed, with the amount of EqtII extending across the membrane being essentially identical to the wild-type protein, to within experimental error. This very strongly supports the role of α-helix dissociation as a pre-requisite for membrane insertion and ultimately pore formation.

In SM- and Chol-containing membranes, the inactive, oxidized EqtII^{V8C,K69C}O mutant shows more of a concentration dependence than the wild-type protein, as documented in Table 4. At 0.05 mg/mL, the amount of EqtII^{V8C,K69C}O adsorbed on the membrane is low, and the layer thickness is only 20±3 Å. At this concentration, no EqtII^{V8C,K69C}O can be detected penetrating into the lipid head groups, but at higher concentrations the amount in the head groups increases in proportion to the total amount of protein, which also displaces solvent from the headgroups. This leads to an apparent shift in the lipid headgroup position in the scattering length density profile in Figure 5d, which, however, corresponds only to the changes in scattering length density/solvent penetration in this region. Above 0.1 mg/mL, the thickness of the EqtII^{V8C,K69C}O layer is constant at 45±4 Å, and, although the amount of protein increases with concentration, at each step up to 50 % of the protein was removed upon changing to a pure buffer solution, indicating partially reversible binding.

4. Discussion

Our neutron reflection results reveal several new details about the membrane binding process of EqtII as a result of the sensitivity of the method to the location, dimensions and amount of protein at the membrane interface, as well as the ability to observe structural changes taking place in the lipid matrix (Fig. 7). The phospholipid DMPC was chosen to allow us to observe the initial stages of EqtII binding and penetration, as the toxin has lower binding and permeabilising activity towards DMPC membranes than corresponding membranes formed with unsaturated phospholipids, such as DOPC [65]. We also verified this by measuring the residual haemolytic activity of unbound EqtII after mixing it with lipid vesicles of different lipid composition. It is clear that vesicles composed of DMPC and its various mixtures with SM and Chol do not promote efficient membrane binding to the extent observed with vesicles that contain the unsaturated lipid DOPC (Fig. S3, Supplementary material).

The perturbation by EqtII of model lipid membranes composed of PC and SM has previously been investigated using solid-state NMR and electron microscopy [70, 71], which showed that the toxin enhanced slow motions in the membrane lipids and destabilized membranes containing SM, suggesting a preferential interaction between the toxin and SM. High-resolution ^{19}F NMR studies [72] shed further light on the interaction, with binding to PC micelles and bicelles causing significant perturbation of resonances from Trp112 and 116 and to a lesser extent Trp117. Subsequent interaction with SM caused further distinct changes, but the interaction with SM was not sufficient to trigger dissociation of the N-terminal helix from the β-sandwich [72].

Our results indicate that EqtII binds peripherally and weakly to pure DMPC. SM promotes the binding of EqtII and induces a change in the protein orientation on the membrane surface; the extension of the toxin outside the lipid surface doubles upon introducing 20 mol% SM. This corresponds more closely to the model of SM-bound EqtII, and actinoporins in general, where the protein interacts with SM through aromatic amino acid residues Trp112 and Tyr113 located in loop at the end of the long axis of the molecule and on the C-terminal α-helix [64]. Such an interaction should reorient the protein in a more vertical orientation, with its long axis approximately perpendicular to the plane of the membrane. This also correlates well with the distinct effect of SM observed on the key Trp residues by ^{19}F NMR [72]. The fraction of EqtII penetrating into the lipid head groups is modest both with and without SM, corresponding to a

significantly smaller part of the protein than the predicted α-helical content, from which we can infer that, in the absence of Chol, α-helix dissociation has not occurred on these membranes.

A modest amount of Chol (10 mol%) gives rise to EqtII penetration all the way across the outer lipid head groups and the membrane hydrophobic core, which has a thickness of 30±1 Å. The helix is proposed to consist of 30 residues once in a membrane, which is long enough to span the membrane. The orientation of the protein remaining outside the membrane remains similar to that in the presence of SM alone. No water is observed to penetrate the membrane to within the experimental detection limit (±3 v/v% relative to the lipids), indicating that no open pores are formed, and the addition of further SM only promotes the binding and penetration of more EqtII, but still without water penetration. This type of initial penetration has been proposed recently to be an intermediate step in the EqtII pore formation process, preceding the oligomerization of several EqtII helices into an open pore within the membrane [39].

Although SM in PC membranes alone has been observed to lead to EqtII insertion and pore formation [73], and EqtII also exhibits some activity in Chol-PC mixtures, the permeabilizing activity strongly depends on the proportions of each lipid in a way that can be related to the phase coexistence regions in the lipid mixtures. In our case, the phase diagram of DMPC, SM and Chol has a relatively small phase coexistence region at much higher SM and Chol fractions than those used in this study [68]. The membrane compositions in our study correspond to a uniform phase, which is fluid at 30 °C and in the gel phase at 18 °C. However, a transition between these two temperatures involves the formation of domains. The observation that cooling the DMPC-SM-Chol-EqtII assembly to 18 °C *in situ* induced a significant amount of water penetration across the membranes supports the proposed role for lipid phase separation in actinoporin pore formation [74, 75], and the affinity of EqtII for lipid microdomains in the plasma membrane [76].

We have shown that EqtII has several different modes of binding to lipid membranes prior to pore formation, suggesting that the orientation of the protein before insertion is different in pure PC membranes compared to SM- or SM- and Chol-containing systems. The existence of a non-pore form of EqtII that spans the lipid membrane is consistent with the proposed mechanism of pore formation, and is also interesting from the point of view of having a less

toxic form of the protein for SM-imaging applications in live cells using GFP [77]. The double cysteine mutant of EqtII binds to all membranes with a similar affinity to the wild-type protein, but shows no penetration into the lipid chains. Releasing the α-helix *in situ* by DTT in the presence of Chol causes full penetration of the protein across the lipid core in a manner which is essentially identical to the wild-type protein. This strongly supports the key role of helix dissociation in pore formation.

5. Conclusions

By using neutron reflection, we have elucidated the structures of membranes interacting with the actinoporin EqtII. We have shown that EqtII binds in several distinct orientations depending on membrane lipid composition, which has not been observed previously. We also show that Chol is required for the penetration of the α-helix across the lipid bilayer, which occurs prior to pore formation at relatively low SM and Chol contents. We show that an intermediate state of EqtII inserts deeply into membranes without pore formation, which is dependent on lipid phase separation, and suggests that membrane domains play a role in the mechanism of EqtII pore formation. Through the use of a double cysteine mutant, we have directly confirmed the role of α-helix dissociation as a pre-requisite for membrane penetration. Our results demonstrate the effectiveness of *in situ* structure determination using neutron reflection and form the basis for more detailed studies of the effects of lipid composition on actinoporin interactions and pore formation in membranes.

Tables

Table 1

Structure of supported lipid bilayers before interaction with EqtII*

	DMPC	20% SM	30% SM	20%SM 10% Chol	30% SM 10% Chol
Membrane thickness (Å)	41±2	44±2	44±2	47±2	46±2
Lipid area per molecule ($Å^2$)	61.5±6	61±6	61±6	57.5±5	54.5±5
% solvent in head groups	18.5±10	36.5±10	33±10	35±10	28±10
% solvent in chains	6±5	0±5	6±5	4±5	1±5

* these values are the average of all prepared bilayers, for which the full data can be found in the Supplementary material.

Table 2

Structure of supported lipid bilayers after introduction of EqtII*

	DMPC	20% SM[#]	30% SM	20% SM 10% Chol	30% SM 10% Chol
Membrane thickness (Å)	39±2	41±2	42±2	47±2	46±2
Lipid area per molecule ($Å^2$)	61±6	63±5	60±5	54±5	53±5
% solvent in head groups	19.5±10	38±10[i] 25±10[o]	32±10[i] 28±10[o]	35±10[i] 40±10[o]	22±10
% solvent in chains	2±5	0±5	0±5	2.5±5	0±5
EqtII μMol m^{-2}	0.13 ±0.03	0.23 ±0.03	0.42 ±0.07	0.30±0.09	0.34±0.10
EqtII layer (Å)	15±3	31±3	27±3	33±3	30±3
v/v% Eqt[$]	6±3	10±5	16±5	10±5	13±5
EqtII depth (Å)	7±3	8±3	8±3	39±3	38±3
v/v% Eqt in lipid heads[¶]	12.5±3	15±3	37±6	10±3	20±3
v/v% Eqt in lipid chains[¶]	-	-	-	11±3	17±3

* these values are the average of all prepared bilayers

[#]Values from experiments with D_{54}-DMPC only when no multilayer formation was observed

[i] inner head groups facing the silicon oxide

[o] outer head groups facing the solution

[$] Volume fraction of protein relative to water

[¶] Volume fraction of protein relative to lipids

Table 3

Membrane structure upon addition of 0.5 mg/mL EqtII at 30 °C and after cooling the membrane-EqtII assembly to 18 °C.

20% SM 10% Chol	0.5mg/mL 30°C	0.5mg/mL 18°C
Membrane thickness (Å)	47±2	51±2
Lipid area per molecule ($Å^2$)	55±5*	61±6*
% solvent in head groups	30±10	19±10 i 14±10 o
% solvent in chains	5±5	22±5
EqtII μMol m^{-2}	0.067±0.016	0.049±0.017
EqtII layer (Å)	35±3	16±3
v/v% Eqt	24±5	39±5
EqtII depth (Å)	38±3	43±3
v/v% Eqt in lipid heads	13±5	38±5
v/v% Eqt in lipid chains	25±2	25±5

*wet area per lipid including the area occupied the solvent.

Table 4

Effect of EqtII-WT and EqtII^{V8C,K69C}O concentration on binding to DMPC-20 mol% SM-10 mol% Chol bilayers.

	EqtII-WT			EqtII^{V8C,K69C}		
EqtII mg/mL	0.05	0.25	0.5	0.05	0.25	0.5
Membrane thickness (Å)	49.5±2	49±2	50±2	48±2	54±2	50±2
Lipid area per molecule (Å^2)	55±5	55±5	53±5	57.5±5	55.5±5	55.5±5
% solvent in head groups	35±10	35±10	35±10	32±10 i 29±10 o	32±10	38.5±10 i 28±10 o
% solvent in lipid chains	4±5[#]	4±5	4±5	5±5	1.5±5	0±5
EqtII thickness (Å)	71±4	71±4	71±4	20±3	47±3	45±3
EqtII penetration depth/Å[§]	41±4	41±4	41±4	0±3	12±3	10±3
v/v% EqtII outside membrane[$]	7±3	4±3	5±3	6±3	6±3	12.5±3
v/v% EqtII in lipid head groups[¶]	8±6	12.5±6	10±6	-	43±6	43±6
v/v % EqtII in lipid chains[¶]	8.5±3	10.5±3	17±3	-	-	-

[#] the lipid bilayers had a chain solvent fraction of 4±5 before introduction of the proteins

[*] measured with protein solution in contact with membrane[/**] after exchanging to pure buffer

[§] The total thickness of the lipid head group and chain regions in which an SLD change was observed

[$] Volume fraction of protein relative to water

[¶] Volume fraction of protein relative to lipids

Table 5

Binding of EqtII^{V8C,K69C}O to DMPC, DMPC-20 mol% SM and DMPC-20 mol% SM-10 mol% Chol membranes before and after conversion into EqtII^{V8C,K69C}R by 2 mM DTT.

	DMPC	DMPC + DTT	20% SM	20% SM+ DTT	20%SM 10% Chol	20%SM 10% Chol+ DTT
Membrane thickness /Å	40±2		43±2	43±2	44±2	44±2
Lipid area per molecule /Å	61±5		63±6	63±6	58±5	58±5
% solvent in head groups	25±10		35±10 i 25±10 o	35±10 i 25±10 o	32±10 i 25±10 o	35±10 i 22±10 o
% solvent in chains	0±5		10±5	10±5	0±5	0±5
EqtII μMol m^{-2}	0.02±0.01		0.03±0.01	0.02±0.01	0.05±0.01	0.05±0.01
EqtII thickness/Å	30±3		38±3	31±3	48±3	71±3
v/v% Eqt outside[$] membrane	7±3		14±5	10±5	20±5	15±5
EqtII penetration depth/Å[§]	-		8±3	8±3	8±3	36±3
v/v% Eqt in lipid head groups[¶]	-		12.5	12.5	11±3	33±3
v/v % Eqt in lipids chains[¶]	-	-	-	-	-	7.5±3

i head groups facing towards silica support

o head groups facing towards solution

[$] Volume fraction of protein relative to water

[§] The total thickness of the lipid head group and chain regions in which an SLD change was observed

[¶] Volume fraction of protein relative to lipids

Legends to figures

Fig. 1. *Schematic representation of the structural model and contrasts used to fit data from lipid bilayers before and after interaction with EqtII.*
Red represents deuterium labelling and blue unlabelled material.

Fig. 2. *Interaction of EqtII with DMPC and D_{54}-DMPC membranes*
a) Neutron reflectivity profiles of DMPC and D_{54}-DMPC membranes before and after EqtII injection at 0.1 mg/mL in H_2O and D_2O, represented as the Fresnel reflectivity RQ^4. The solid lines show the best fit to the data corresponding to the scattering length density (SLD) profiles in b), which also shows a schematic illustration of the EqtII location and possible orientations at the membrane-water interface. Sensitivity of the fit to c) the presence of solvent in the lipid bilayer – the black solid line shows a change of 3v/v% D_2O in the lipid chains - and d) the penetration of EqtII into the lipid hydrocarbon chains – the solid black line shows a change in the lipid chain scattering length density by the -0.1×10^{-6} Å^{-2} corresponding to the penetration of 3 v/v% of H-Eqt in the deuterated lipid chains.

Fig. 3. *Interaction of EqtII with DMPC and D_{54}-DMPC membranes containing SM*
Neutron reflectivity profiles of D_{54}-DMPC membranes with a) 20 mol% and c) 30 mol% SM before and after EqtII injection at 0.1 mg/mL in H_2O and D_2O. The solid lines show the best fit to the data corresponding to the scattering length density (SLD) profiles in b) and d), which also indicate the EqtII location and possible orientations at the membrane-water interface.

Fig. 4. *Interaction of EqtII with DMPC and D_{54}-DMPC membranes containing SM and Chol*
Reflectivity profiles and scattering length density profiles and model structures (Table 3) of D_{54}-DMPC membranes with 10 mol% Chol and a,b) 20 mol% or c,d) 30 mol% SM before and after EqtII injection at 0.1 mg/mL in H_2O and D_2O. b,d) Illustration of EqtII location and possible orientations of the embedded α-helix. The green EqtII cartoons in b) illustrate the membrane thickening and aqueous pore formation that occurs upon cooling the membrane-EqtII assembly to 18 °C, crossing the gel-phase boundary.

Fig. 5. *Association of EqtII and EqtII^{V8C,K69C}O at different protein concentration*

Reflectivity profiles (plotted as normalised reflectivity RQ^4 to emphasize differences in the membrane reflectivity) and neutron scattering length density profiles illustrating the model structures (4) fitted for DMPC-20 mol% SM 10%Chol as function of a,b) H-Eqt-WT concentration and c,d) EqtII^{V8C,K69C}O concentration in H_2O and D_2O.

Fig. 6. *Interaction of D-EqtII^{V8C,K69C}O with membranes*

Reflectivity profiles and neutron scattering length density profiles of a,b) DMPC, c,d) DMPC-20 mol% SM and e,f) DMPC-20mol% SM-10 mol% Chol membranes before and after EqtII^{V8C,K69C}O injection at 0.1 mg/mL in H_2O and D_2O. f) illustrates the penetration of the protein that occurs upon addition of 2 mM DTT in the presence of Chol.

Fig. 7. *Schematic summary of the binding of EqtII-WT and EqtII^{V8C,K69C}O to lipid bilayers.*

Acknowledgements

The authors thank the Institut Laue-Langevin for the experimental neutron beam time, the provision of deuterated protein, a as well as use of the supporting facilities of the Partnership for Soft Condensed Matter. V.T.F. and M.H. acknowledge support from the UK EPSRC under grants GR/R99393/01 and EP/C015452/1 for the development of the Deuteration Laboratory at the ILL. This work was supported in part by the Access to Major Research Facilities Program administered by ANSTO and the Slovenian Research Agency. R.S.N. acknowledges fellowship support from the Australian National Health and Medical Research Council.

References

[1] G. Anderluh, P. Maček, Cytolytic peptide and protein toxins from sea anemones (Anthozoa: Actiniaria), Toxicon, 40 (2002) 111-124.

[2] K. Črnigoj Kristan, G. Viero, M. Dalla Serra, P. Maček, G. Anderluh, Molecular mechanism of pore formation by actinoporins, Toxicon, 54 (2009) 1125-1134.

[3] L. Garcia-Ortega, J. Alegre-Cebollada, S. Garcia-Linares, M. Bruix, A. Martinez-Del-Pozo, J.G. Gavilanes, The behavior of sea anemone actinoporins at the water-membrane interface, Biochim. Biophys. Acta, 1808 (2011) 2275-2288.

[4] G. Anderluh, J.H. Lakey, Disparate proteins use similar architectures to damage membranes, Trends Biochem. Sci., 33 (2008) 482-490.

[5] R.J. Gilbert, M. Dalla Serra, C.J. Froelich, M.I. Wallace, G. Anderluh, Membrane pore formation at protein-lipid interfaces, Trends Biochem. Sci., 39 (2014) 510-516.

[6] G. Belmonte, C. Pederzolli, P. Maček, G. Menestrina, Pore formation by the sea anemone cytolysin equinatoxin II in red blood cells and model lipid membranes, J. Membr. Biol., 131 (1993) 11-22.

[7] V. de los Rios, J.M. Mancheno, A. Martinez del Pozo, C. Alfonso, G. Rivas, M. Onaderra, J.G. Gavilanes, Sticholysin II, a cytolysin from the sea anemone *Stichodactyla helianthus*, is a monomer-tetramer associating protein, FEBS Lett., 455 (1999) 27-30.

[8] G. Anderluh, A. Barlič, C. Potrich, P. Maček, G. Menestrina, Lysine 77 is a key residue in aggregation of equinatoxin II, a pore-forming toxin from sea anemone *Actinia equina*, J. Membr. Biol., 173 (2000) 47-55.

[9] M. Tejuca, M. Dalla Serra, C. Potrich, C. Alvarez, G. Menestrina, Sizing the radius of the pore formed in erythrocytes and lipid vesicles by the toxin sticholysin I from the sea anemone *Stichodactyla helianthus*, J. Membr. Biol., 183 (2001) 125-135.

[10] M. Tejuca, M. Dalla Serra, M. Ferreras, M.E. Lanio, G. Menestrina, Mechanism of membrane permeabilization by sticholysin I, a cytolysin isolated from the venom of the sea anemone *Stichodactyla helianthus*, Biochemistry, 35 (1996) 14947-14957.

[11] M.A. Baker, N. Rojko, B. Cronin, G. Anderluh, M.I. Wallace, Photobleaching reveals heterogeneous stoichiometry for equinatoxin II oligomers, Chembiochem, 15 (2014) 2139-2145.

[12] Y. Subburaj, U. Ros, E. Hermann, R. Tong, A.J. Garcia-Saez, Toxicity of an α-pore-forming toxin depends on the assembly mechanism on the target membrane as revealed by single-molecule imaging, J. Biol. Chem., 290 (2015) 4856-4865.

[13] J.M. Mancheno, J. Martin-Benito, M. Martinez-Ripoll, J.G. Gavilanes, J.A. Hermoso, Crystal and electron microscopy structures of sticholysin II actinoporin reveal insights into the mechanism of membrane pore formation, Structure, 11 (2003) 1319-1328.

[14] A.E. Mechaly, A. Bellomio, D. Gil-Carton, K. Morante, M. Valle, J.M. Gonzalez-Manas, D.M. Guerin, Structural insights into the oligomerization and architecture of eukaryotic membrane pore-forming toxins, Structure, 19 (2011) 181-191.

[15] K. Tanaka, J.M. Caaveiro, K. Morante, J.M. Gonzalez-Manas, K. Tsumoto, Structural basis for self-assembly of a cytolytic pore lined by protein and lipid, Nature Comm., 6 (2015) 6337.

[16] A.W. Bernheimer, L.S. Avigad, Properties of a toxin from the sea anemone *Stoichacis helianthus*, including specific binding to sphingomyelin, Proc. Natl. Acad. Sci. U. S. A, 73 (1976) 467-471.

[17] R. Linder, A.W. Bernheimer, K.S. Kim, Interaction between sphingomyelin and a cytolysin from the sea anemone *Stoichactis helianthus*, Biochim. Biophys. Acta, 467 (1977) 290-300.

[18] V. de los Rios, J.M. Mancheno, M.E. Lanio, M. Onaderra, J.G. Gavilanes, Mechanism of the leakage induced on lipid model membranes by the hemolytic protein sticholysin II from the sea anemone *Stichodactyla helianthus*, Eur. J. Biochem., 252 (1998) 284-289.

[19] R.J. Simpson, G.E. Reid, R.L. Moritz, C. Morton, R.S. Norton, Complete amino acid sequence of tenebrosin-C, a cardiac stimulatory and haemolytic protein from the sea anemone *Actinia tenebrosa*, Eur. J. Biochem., 190 (1990) 319-328.

[20] R.S. Norton, G. Bobek, J.O. Ivanov, M. Thomson, E. Fiala-Beer, R.L. Moritz, R.J. Simpson, Purification and characterisation of proteins with cardiac stimulatory and haemolytic activity from the anemone *Actinia tenebrosa*, Toxicon, 28 (1990) 29-41.

[21] R.S. Norton, P. Maček, G.E. Reid, R.J. Simpson, Relationship between the cytolysins tenebrosin-C from *Actinia tenebrosa* and equinatoxin II from *Actinia equina*, Toxicon, 30 (1992) 13-23.

[22] P. Galettis, R.S. Norton, Biochemical and pharmacological studies of the mechanism of action of tenebrosin-C, a cardiac stimulatory and haemolytic protein from the sea anemone, *Actinia tenebrosa*, Toxicon, 28 (1990) 695-706.

[23] P. Maček, D. Lebez, Isolation and characterization of three lethal and hemolytic toxins from the sea anemone *Actinia equina* L, Toxicon, 26 (1988) 441-451.

[24] B. Bakrač, G. Anderluh, Molecular mechanism of sphingomyelin-specific membrane binding and pore formation by actinoporins, Adv. Exp. Med. Biol., 677 (2010) 106-115.

[25] T. Maula, Y.J. Isaksson, S. Garcia-Linares, S. Niinivehmas, O.T. Pentikainen, M. Kurita, S. Yamaguchi, T. Yamamoto, S. Katsumura, J.G. Gavilanes, A. Martinez-del-Pozo, J.P. Slotte, 2NH and 3OH are crucial structural requirements in sphingomyelin for sticholysin II binding and pore formation in bilayer membranes, Biochim. Biophys. Acta, 1828 (2013) 1390-1395.

[26] G. Belmonte, G. Menestrina, C. Pederzolli, I. Križaj, F. Gubenšek, T. Turk, P. Maček, Primary and secondary structure of a pore-forming toxin from the sea anemone, *Actinia equina* L., and its association with lipid vesicles, Biochim. Biophys. Acta, 1192 (1994) 197-204.

[27] W. Zhang, M.G. Hinds, G. Anderluh, P.E. Hanse, R.S. Norton, Letter to the editor: Sequence-specific resonance assignments of the potent cytolysin equinatoxin II, J Biomol NMR, 18 (2000) 281-282.

[28] M.G. Hinds, W. Zhang, G. Anderluh, P.E. Hansen, R.S. Norton, Solution structure of the eukaryotic pore-forming cytolysin equinatoxin II: implications for pore formation, J. Mol. Biol., 315 (2002) 1219-1229.

[29] A. Athanasiadis, G. Anderluh, P. Maček, D. Turk, Crystal structure of the soluble form of equinatoxin II, a pore-forming toxin from the sea anemone *Actinia equina*, Structure, 9 (2001) 341-346.

[30] N. Poklar, J. Fritz, P. Maček, G. Vesnaver, T.V. Chalikian, Interaction of the pore-forming protein equinatoxin II with model lipid membranes: A calorimetric and spectroscopic study, Biochemistry, 38 (1999) 14999-15008.

[31] G. Menestrina, V. Cabiaux, M. Tejuca, Secondary structure of sea anemone cytolysins in soluble and membrane bound form by infrared spectroscopy, Biochem. Biophys. Res. Commun., 254 (1999) 174-180.

[32] G. Anderluh, A. Barlič, Z. Podlesek, P. Maček, J. Pungerčar, F. Gubenšek, M.L. Zecchini, M. Dalla Serra, G. Menestrina, Cysteine-scanning mutagenesis of an eukaryotic pore-forming toxin from sea anemone: topology in lipid membranes, Eur. J. Biochem., 263 (1999) 128-136.

[33] P. Malovrh, G. Viero, M.D. Serra, Z. Podlesek, J.H. Lakey, P. Maček, G. Menestrina, G. Anderluh, A novel mechanism of pore formation, J. Biol. Chem., 278 (2003) 22678-22685.

[34] P. Malovrh, A. Barlič, Z. Podlesek, P. Maček, G. Menestrina, G. Anderluh, Structure-function studies of tryptophan mutants of equinatoxin II, a sea anemone pore-forming protein, Biochem. J., 346 (2000) 223-232.

[35] Q. Hong, I. Gutierrez-Aguirre, A. Barlič, P. Malovrh, K. Kristan, Z. Podlesek, P. Maček, D. Turk, J.M. Gonzalez-Manas, J.H. Lakey, G. Anderluh, Two-step membrane binding by equinatoxin II, a pore-forming toxin from the sea anemone, involves an exposed aromatic cluster and a flexible helix, J. Biol. Chem., 277 (2002) 41916-41924.

[36] A. Drechsler, C. Potrich, J.K. Sabo, M. Frisanco, G. Guella, M. Dalla Serra, G. Anderluh, F. Separovic, R.S. Norton, Structure and activity of the N-terminal region of the eukaryotic cytolysin equinatoxin II, Biochemistry, 45 (2006) 1818-1828.

[37] K. Kristan, G. Viero, P. Maček, M. Dalla Serra, G. Anderluh, The equinatoxin N-terminus is transferred across planar lipid membranes and helps to stabilize the transmembrane pore, FEBS J., 274 (2007) 539-550.

[38] K. Kristan, Z. Podlesek, V. Hojnik, I. Gutierrez-Aguirre, G. Gunčar, D. Turk, J.M. Gonzalez-Manas, J.H. Lakey, P. Maček, G. Anderluh, Pore formation by equinatoxin, a eukaryotic pore-forming toxin, requires a flexible N-terminal region and a stable β-sandwich, J. Biol. Chem., 279 (2004) 46509-46517.

[39] N. Rojko, K.C. Kristan, G. Viero, E. Žerovnik, P. Maček, M. Dalla Serra, G. Anderluh, Membrane damage by an α-helical pore-forming protein, equinatoxin II, proceeds through a succession of ordered steps, J. Biol. Chem., 288 (2013) 23704-23715.

[40] J.B. Hayter, R.R. Highfield, B.J. Pullman, R.K. Thomas, A.I. McMullen, J. Penfold, Critical reflection of neutrons - a new technique for investigating interfacial phenomena, J. Chem. Soc. Faraday Trans. I, 77 (1981) 1437-1448.

[41] H.P. Wacklin, Interfacial Mechanism of Phospholipase A(2): pH-Dependent Inhibition and Me-β-cyclodextrin Activation, Biochemistry, (2009).

[42] M. Cardenas, H. Wacklin, R.A. Campbell, T. Nylander, Structure of DNA-cationic surfactant complexes at hydrophobically modified and hydrophilic silica surfaces as revealed by neutron reflectometry, Langmuir, 27 (2011) 12506-12514.

[43] A. Michanek, M. Yanez, H. Wacklin, A. Hughes, T. Nylander, E. Sparr, RNA and DNA Association to zwitterionic and charged monolayers at the air liquid interface, Langmuir, 28 (2012) 9621-9633.

[44] H.P. Wacklin, Neutron reflection from supported lipid membranes, Curr. Opin. Colloid Interface Sci., 15 (2010) 445-454.

[45] H.P. Wacklin, Composition and asymmetry in supported membranes formed by vesicle fusion, Langmuir, 27 (2011) 7698-7707.

[46] L.A. Clifton, C.L. Johnson, A.S. Solovyova, P. Callow, K.L. Weiss, H. Ridley, A.P. Le Brun, C.J. Kinane, J.R. Webster, S.A. Holt, J.H. Lakey, Low resolution structure and dynamics of a colicin-receptor complex determined by neutron scattering, J. Biol. Chem., 287 (2012) 337-346.

[47] A. Chenal, L. Prongidi-Fix, A.l. Perier, C. Aisenbrey, G.g. Vernier, S. Lambotte, G. Fragneto, B. Bechinger, D. Gillet, V. Forge, M. Ferrand, Deciphering Membrane Insertion of the Diphtheria Toxin T Domain by Specular Neutron Reflectometry and Solid-State NMR Spectroscopy, J. Mol. Biol., 391 (2009) 872-883.

[48] D.J. McGillivray, G. Valincius, F. Heinrich, J.W.F. Robertson, D.J. Vanderah, W. Febo-Ayala, I. Ignatjev, M. Losche, J.J. Kasianowicz, Structure of Functional *Staphylococcus aureus* α-Hemolysin Channels in Tethered Bilayer Lipid Membranes, Biophys. J., 96 (2009) 1547-1553.

[49] G. Anderluh, J. Pungerčar, B. Štrukelj, P. Maček, F. Gubenšek, Cloning, sequencing, and expression of equinatoxin II, Biochem. Biophys. Res. Commun., 220 (1996) 437-442.

[50] B. Leiting, F. Marsilio, J.F. O'Connell, Predictable Deuteration of Recombinant Proteins Expressed in *Escherichia coli*, Anal. Biochem., 265 (1998) 351-355.

[51] S.L. Grage, A.M. Keleshian, T. Turdzeladze, A.R. Battle, W.C. Tay, R.P. May, S.A. Holt, S.A. Contera, M. Haertlein, M. Moulin, P. Pal, P.R. Rohde, V.T. Forsyth, A. Watts, K.C. Huang, A.S. Ulrich, B. Martinac, Bilayer-mediated clustering and functional interaction of MscL channels, Biophys. J., 100 (2011) 1252-1260.

[52] M.G. Cuypers, S.A. Mason, M.P. Blakeley, E.P. Mitchell, M. Haertlein, V.T. Forsyth, Near-atomic resolution neutron crystallography on perdeuterated *Pyrococcus furiosus* rubredoxin: implication of hydronium ions and protonation state equilibria in redox changes, Angew. Chem. Int. Ed. Engl., 52 (2013) 1022-1025.

[53] N. Brouette, G. Fragneto, F. Cousin, M. Moulin, M. Haertlein, M. Sferrazza, A neutron reflection study of adsorbed deuterated myoglobin layers on hydrophobic surfaces, J. Colloid Inter. Sci., 390 (2013) 114-120.

[54] J.B. Artero, M. Hartlein, S. McSweeney, P. Timmins, A comparison of refined X-ray structures of hydrogenated and perdeuterated rat gammaE-crystallin in H2O and D2O, Acta Crystallogr. D Biol. Crystallogr., 61 (2005) 1541-1549.

[55] D. Bauza, Chapter 2 - Thermal Oxidation of Silicon and Si-SiO2 Interface Morphology, Structure and Localized States, in: H.S. Nalwa (Ed.) Handbook of Surfaces and Interfaces of Materials, Academic Press, Burlington, 2001, pp. 115-216.

[56] A. Akesson, T. Lind, N. Ehrlich, D. Stamou, H. Wacklin, M. Cardenas, Composition and structure of mixed phospholipid supported bilayers formed by POPC and DPPC, Soft Matter, 8 (2012) 5658-5665.

[57] R. Cubitt, G. Fragneto, D17: the new reflectometer at the ILL, Applied Phys. Mat. Sci. Proc., 74 (2002) S329-S331.

[58] H.P. Vacklin, F. Tiberg, G. Fragneto, R.K. Thomas, Composition of supported model membranes determined by neutron reflection, Langmuir, 21 (2005) 2827-2837.

[59] H.P. Vacklin, F. Tiberg, G. Fragneto, R.K. Thomas, Phospholipase A2 hydrolysis of supported phospholipid bilayers: a neutron reflectivity and ellipsometry study, Biochemistry, 44 (2005) 2811-2821.

[60] A. Nelson, Co-refinement of multiple-contrast neutron/X-ray reflectivity data using MOTOFIT, J. Appl. Crystallogr., 39 (2006) 273-276.

[61] R.S. Armen, O.D. Uitto, S.E. Feller, Phospholipid component volumes: Determination and application to bilayer structure calculations, Biophys. J., 75 (1998) 734-744.

[62] A.A. Zamyatin, Protein volume in solution, Prog. Biophys. Mol. Biol., 24 (1972) 107-123.

[63] C.H. Chen, S. Malkova, S.V. Pingali, F. Long, S. Garde, W. Cho, M.L. Schlossman, Configuration of PKCalpha-C2 domain bound to mixed SOPC/SOPS lipid monolayers, Biophys J, 97 (2009) 2794-2802.

[64] B. Bakrač, I. Gutiérrez-Aguirre, Z. Podlesek, A.F.-P. Sonnen, R.J.C. Gilbert, P. Maček, J.H. Lakey, G. Anderluh, Molecular determinants of sphingomyelin specificity of a eukaryotic pore-forming toxin, J. Biol. Chem., 283 (2008) 18665-18677.

[65] A.J. Miles, A. Drechsler, K. Kristan, G. Anderluh, R.S. Norton, B.A. Wallace, F. Separovic, The effects of lipids on the structure of the eukaryotic cytolysin equinatoxin II: a synchrotron radiation circular dichroism spectroscopic study, Biochim. Biophys. Acta, 1778 (2008) 2091-2096.

[66] C. Faure, L. Bonakdar, E.J. Dufourc, Determination of DMPC hydration in the Lα and Lβ′ phases by 2H solid state NMR of D2O, FEBS Lett., 405 (1997) 263-266.

[67] C. Chachaty, D. Rainteau, C. Tessier, P.J. Quinn, C. Wolf, Building up of the liquid-ordered phase formed by sphingomyelin and cholesterol, Biophys. J., 88 (2005) 4032-4044.

[68] N. Kahya, D. Scherfeld, P. Schwille, Differential lipid packing abilities and dynamics in giant unilamellar vesicles composed of short-chain saturated glycerol-phospholipids, sphingomyelin and cholesterol, Chem. Phys. Lipids, 135 (2005) 169-180.

[69] P.F.F. Almeida, A. Pokorny, A. Hinderliter, Thermodynamics of membrane domains, Biochim. Biophys. Acta - Biomembranes, 1720 (2005) 1-13.

[70] G. Anderluh, M. Dalla Serra, G. Viero, G. Guella, P. Maček, G. Menestrina, Pore formation by equinatoxin II, a eukaryotic protein toxin, occurs by induction of nonlamellar lipid structures, J. Biol. Chem., 278 (2003) 45216-45223.

[71] B.B. Bonev, Y.H. Lam, G. Anderluh, A. Watts, R.S. Norton, F. Separovic, Effects of the eukaryotic pore-forming cytolysin equinatoxin II on lipid membranes and the role of sphingomyelin, Biophys. J., 84 (2003) 2382-2392.

[72] G. Anderluh, A. Razpotnik, Z. Podlesek, P. Maček, F. Separovic, R.S. Norton, Interaction of the eukaryotic pore-forming cytolysin equinatoxin II with model membranes: ^{19}F NMR studies, J. Mol. Biol., 347 (2005) 27-39.

[73] J.M. Caaveiro, I. Echabe, I. Gutierrez-Aguirre, J.L. Nieva, J.L. Arrondo, J.M. Gonzalez-Manas, Differential interaction of equinatoxin II with model membranes in response to lipid composition, Biophys. J., 80 (2001) 1343-1353.

[74] A. Barlič, I. Gutiérrez-Aguirre, J.M.M. Caaveiro, A. Cruz, M.-B. Ruiz-Argüello, J. Pérez-Gil, J.M. González-Mañas, Lipid Phase Coexistence favors membrane insertion of equinatoxin-ii, a pore-forming toxin from Actinia equina, J. Biol. Chem., 279 (2004) 34209-34216.

[75] N. Rojko, B. Cronin, J.S. Danial, M.A. Baker, G. Anderluh, M.I. Wallace, Imaging the lipid-phase-dependent pore formation of equinatoxin II in droplet interface bilayers, Biophys. J., 106 (2014) 1630-1637.

[76] A.J. García-Sáez, S.B. Buschhorn, H. Keller, G. Anderluh, K. Simons, P. Schwille, Oligomerization and pore formation by equinatoxin ii inhibit endocytosis and lead to plasma membrane reorganization, J. Biol. Chem., 286 (2011) 37768-37777.

[77] B. Bakrač, A. Kladnik, P. Maček, G. McHaffie, A. Werner, J.H. Lakey, G. Anderluh, A toxin-based probe reveals cytoplasmic exposure of Golgi sphingomyelin, J. Biol. Chem., 285 (2010) 22186-22195.

Figures

Figure 1

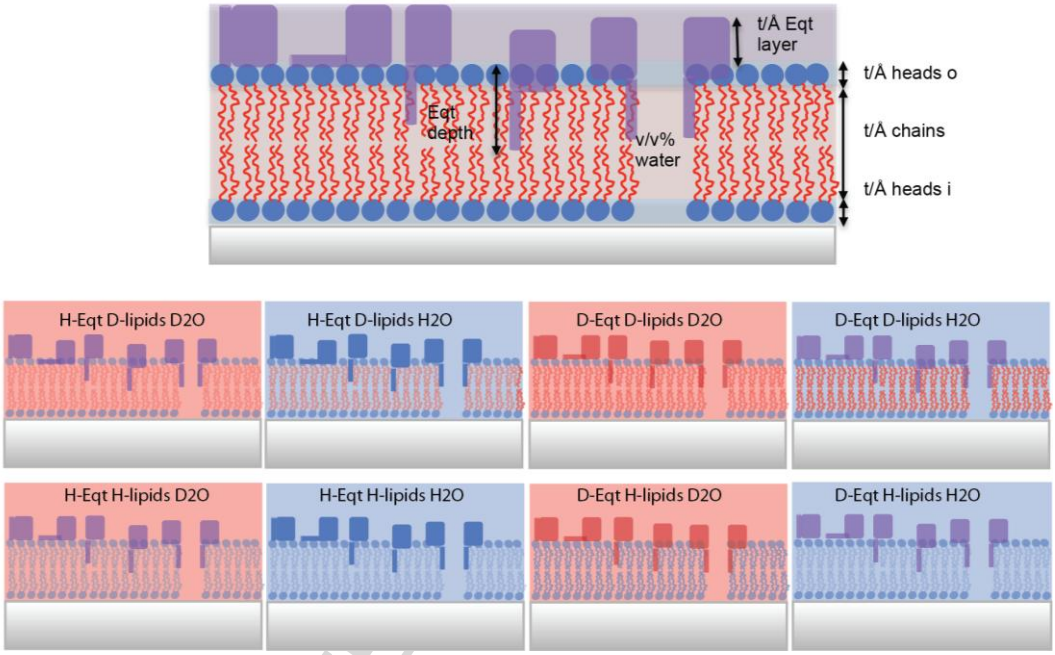

Figure 2

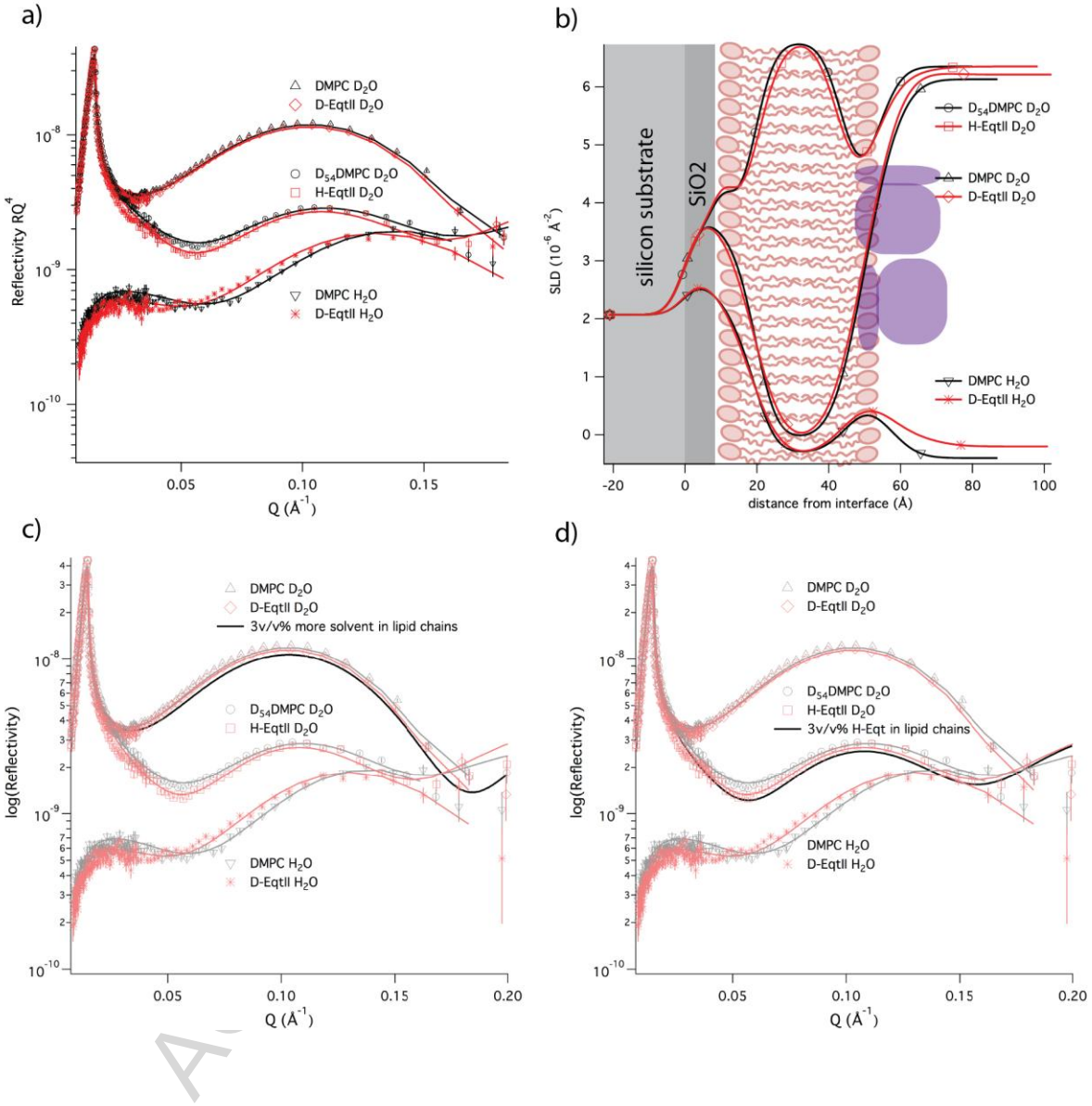

Figure 3

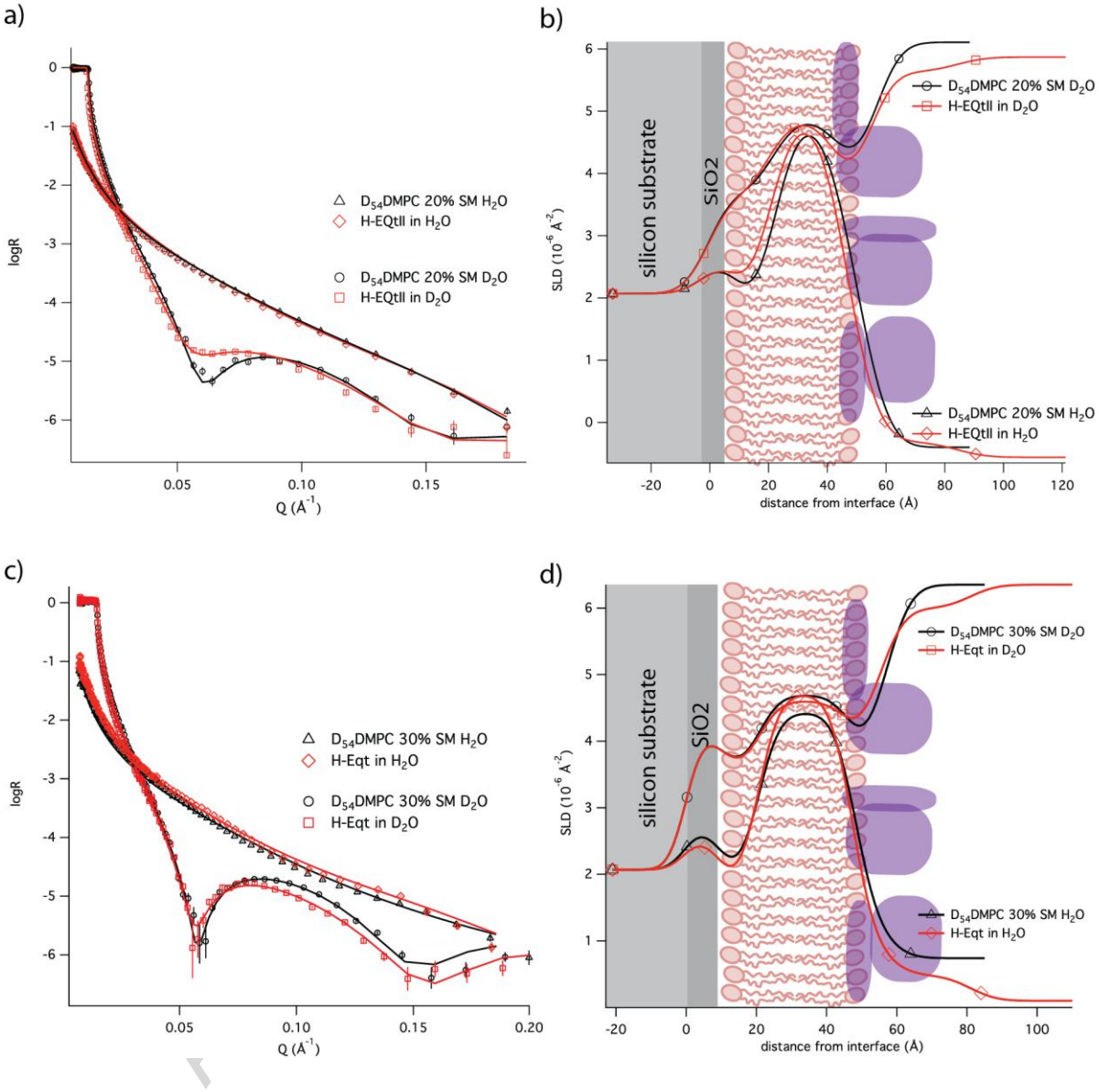

Figure 4

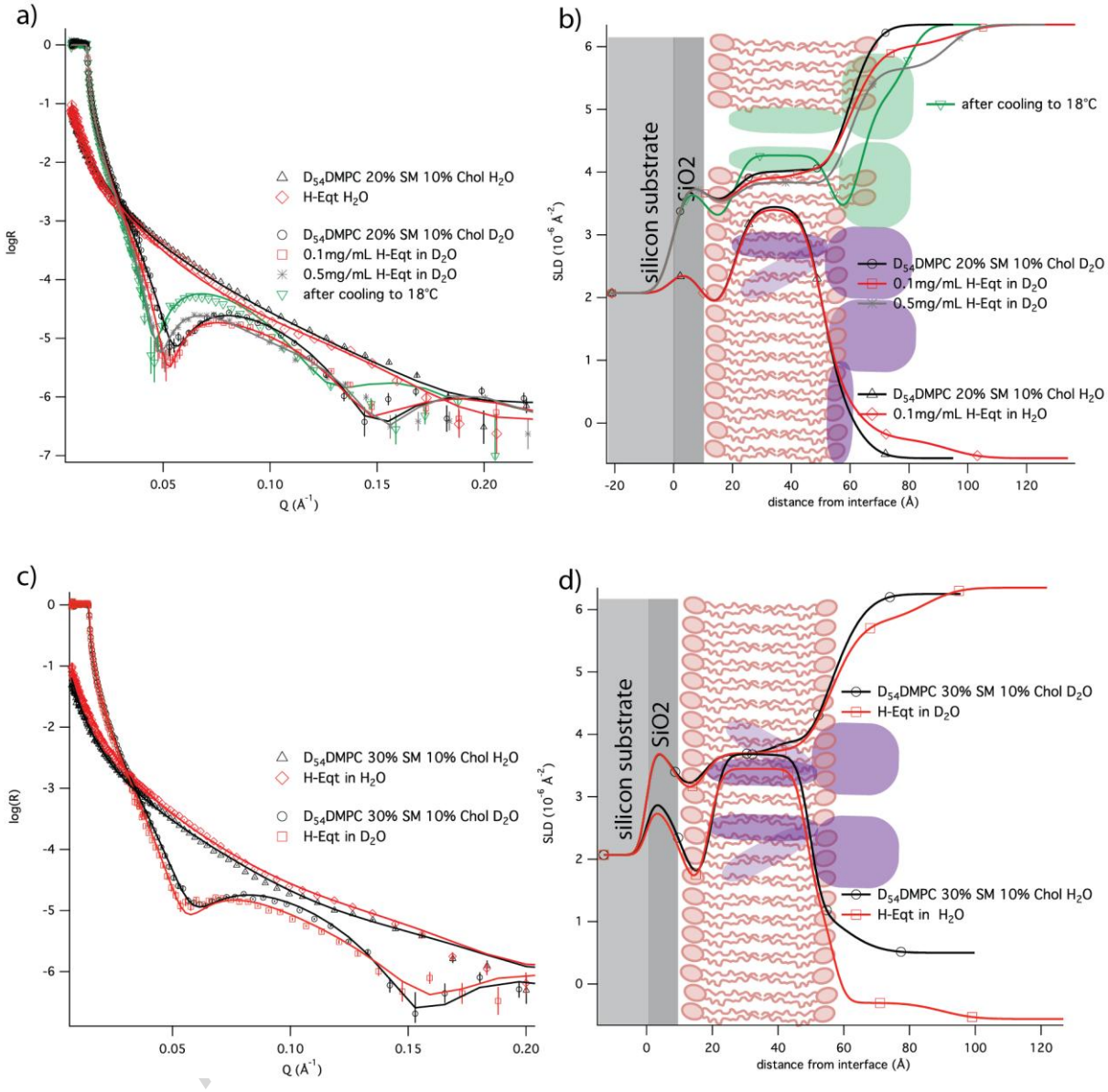

Figure 5

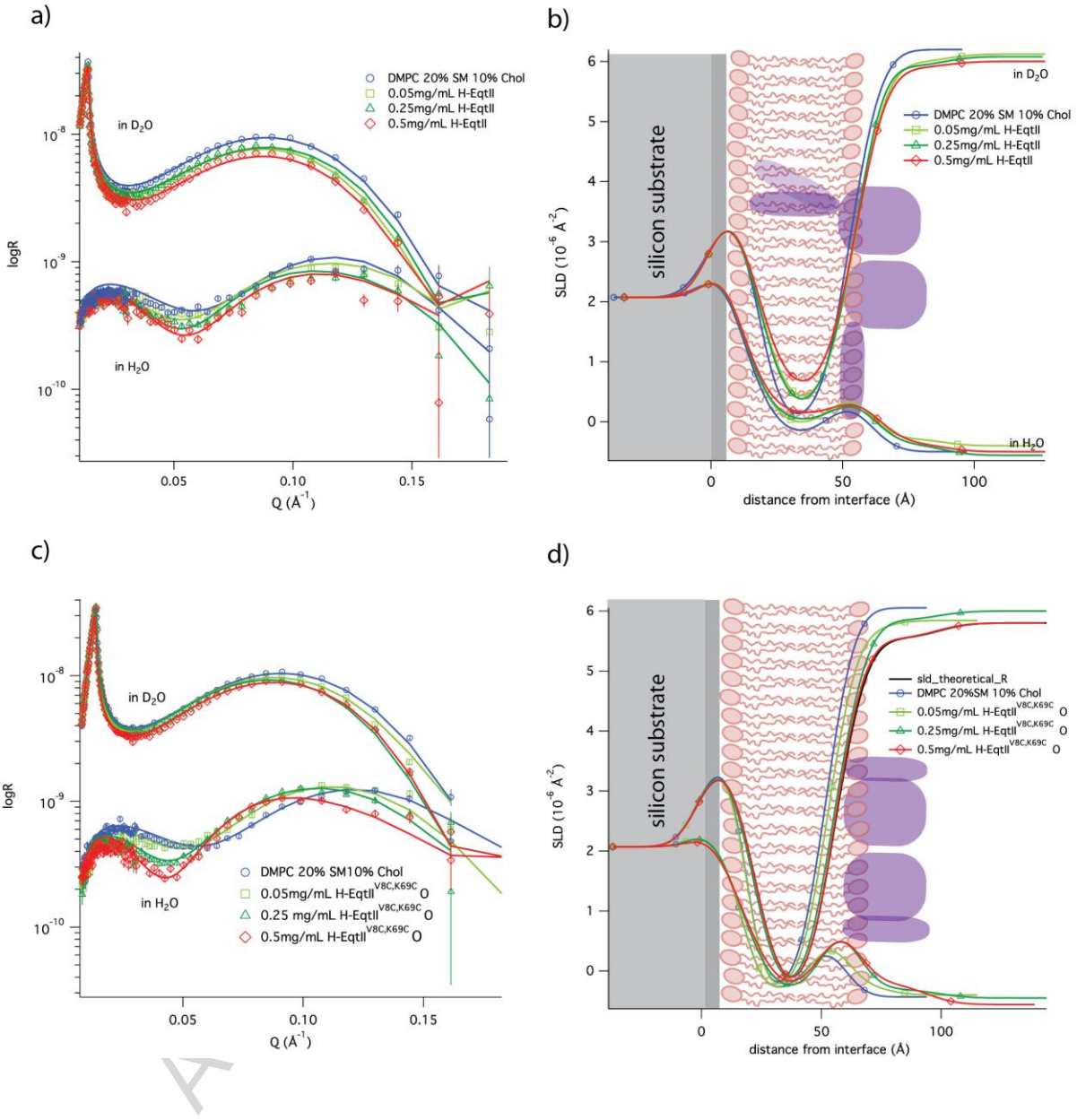

Figure 6

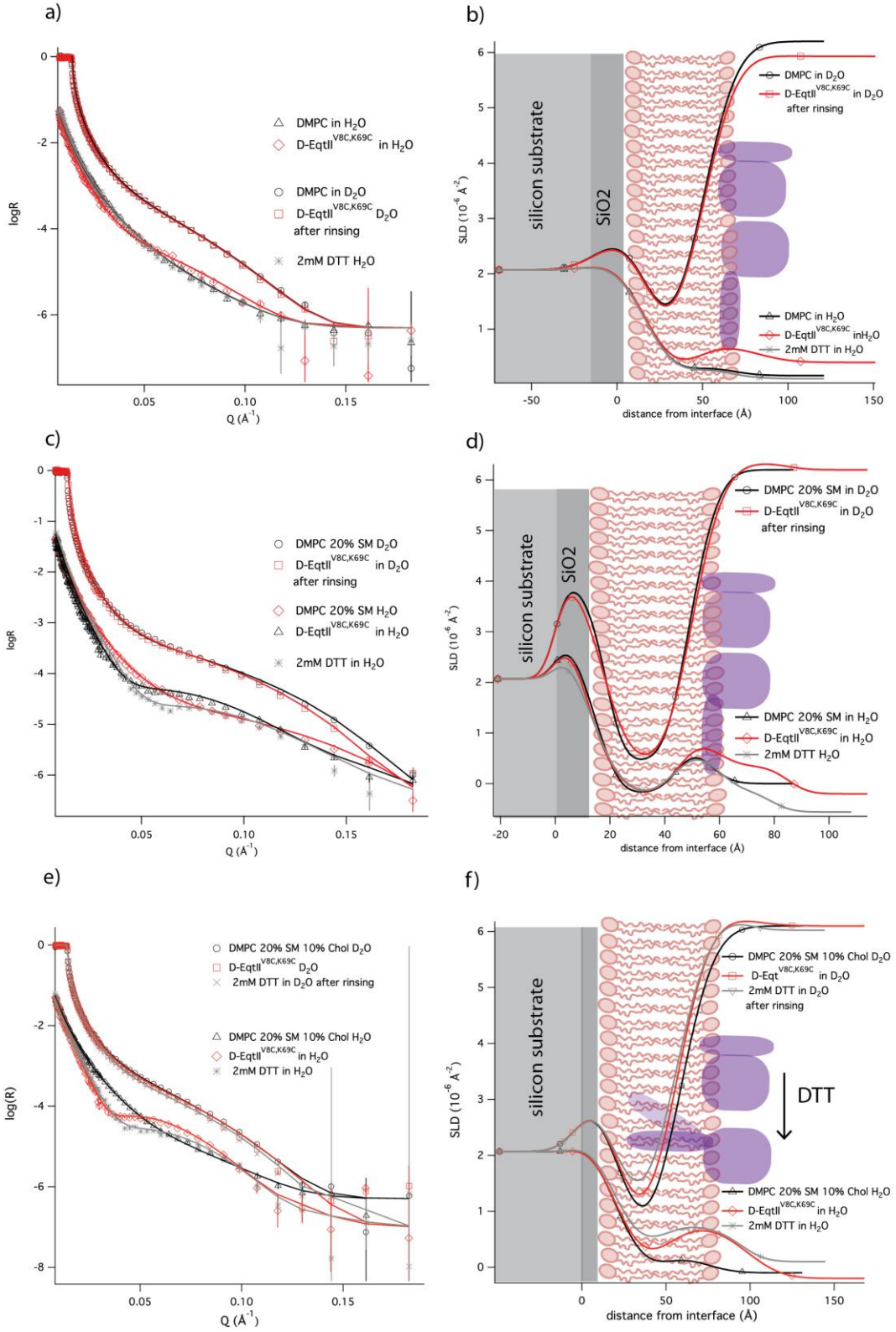

Figure 7

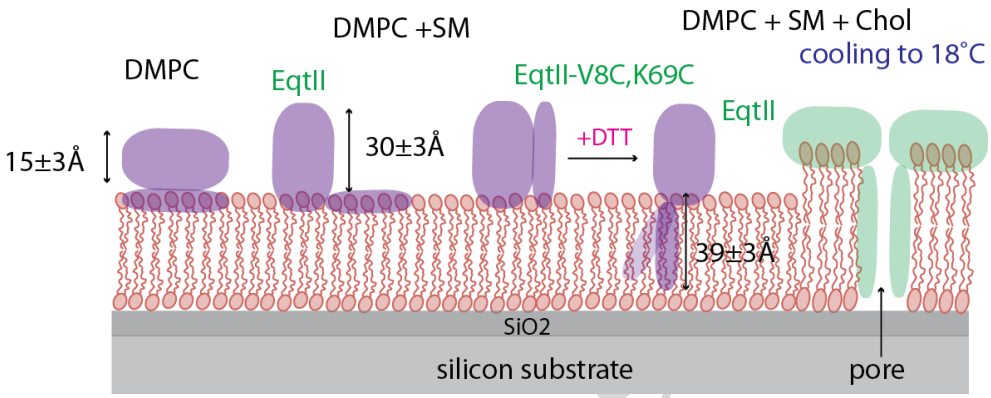

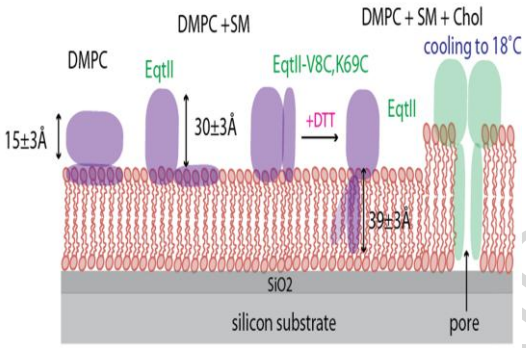

Graphical abstract

Highlights

- Equinatoxin II has several modes of membrane binding depending on lipid composition
- Equinatoxin II binds in a different orientation to DMPC-sphingomyelin compared with pure DMPC
- Phase-separation promotes pore formation in DMPC-SM-cholesterol membranes
- *In situ* release of the N-terminal α-helix confirms its role in pore formation